Progress in ultrafast, mid-infrared optical parametric chirped pulse amplifiers pumped at 1 µm

Mark Mero*[a], Valentin Petrov[a], Zsuzsanna Heiner[§b]
[a]Max Born Institute for Nonlinear Optics and Short Pulse Spectroscopy, 12489 Berlin, Germany;
[b]School of Analytical Sciences Adlershof SALSA, Humboldt-Universität zu Berlin, 12489 Berlin, Germany

ABSTRACT

With diode-pumped Yb laser technology reaching maturity, average power scaling of multi-GW, few-cycle, short-wave and mid-infrared (MIR) optical parametric amplifiers (OPA's) to the 100-W level has become a reality. Well established, commercially available oxide crystals offer a relatively straightforward solution in the 1.4-4-µm spectral range. Extension of the spectral coverage of high-power OPA's beyond 5 µm may be enabled by novel, wide-bandgap non-oxide crystals with growth processes still under major development and optimization. Here, we present our results on the nonlinear optical properties of oxide ($LiNbO_3$, $KTiOAsO_4$) and non-oxide ($LiGaS_2$, $BaGa_4S_7$) crystals and the resulting 100-kHz, ultrafast infrared OPA's based on these materials. The reported data provide design parameters and guidelines for high-average-power MIR OPA's pumped by Yb lasers both below and above 5 µm.

Keywords: Nonlinear optical crystals, OPCPA, photorefractive damage, z-scan, nonlinear refractive index, $KTiOAsO_4$, $LiGaS_2$, $BaGa_4S_7$

1. INTRODUCTION

Diode-pumped ps and sub-ps Yb lasers are rapidly taking the place of Ti:sapphire lasers as pump sources in ultrafast optical parametric amplifiers (OPA's) and optical parametric chirped pulse amplifiers (OPCPA's). Importantly, Yb lasers have recently enabled unprecedented average powers from OPCPA's operating in the short-wave infrared (SWIR, 1.4-3 µm) and at the blue edge of the mid-infrared (MIR, 3-30 µm). In the 1.4-4 µm wavelength region, where a number of wide-bandgap oxide nonlinear optical crystals are commercially available, multi-GW peak powers at average powers well above 10 W have already been demonstrated with pulses lasting only a few optical cycles. Most of the demonstrated high-power OPA systems relied on bulk, critically phase-matched crystals for power scaling,[1-4] such as $KNbO_3$, $LiNbO_3$, and $KTiOAsO_4$ (KTA), while only one utilized periodically poled $LiNbO_3$ (PPLN) for this purpose.[5]

Due to the lack of suitable nonlinear crystals, ultrafast optical parametric devices operating beyond 5 µm were based almost exclusively on an OPA followed by difference frequency generation (DFG) at an overall pump-to-MIR energy conversion efficiency below 1% at 8 µm. Recent progress in the manufacture of wide-bandgap non-oxide nonlinear crystals with high quality and size shows great promise for power-scalable MIR OPA's pumped directly at 1 µm with negligible two-photon absorption. As a DFG module is not needed in this case to reach wavelengths above 5 µm, the conversion efficiency can be significantly boosted in the 5-10 µm range compared to the traditional cascaded OPA-DFG scheme.

Two examples of wide-bandgap non-oxide crystals with their growth process under development are LGS ($LiGaS_2$) and BGS ($BaGa_4S_7$). While the nonlinear coefficient and figure of merit of these materials are the lowest among birefringent non-oxide crystals, their melting temperature, hardness, thermal conductivity, and resistance to laser-induced damage are the highest.[6] The latter properties together with negligible two-photon absorption at 1 µm offer significant advantage in high-power ultrafast MIR OPA's. Compared to the commercially available non-oxide crystal $AgGaS_2$, which can be considered as a benchmark material for MIR OPA's pumped at 1 µm, both LGS and BGS offer wider bandgap and better thermo-mechanical and laser damage properties albeit at lower figure of merit. Although single-crystal LGS has been grown for decades,[7] obtaining large sizes for this material at high quality is difficult. BGS shows great promise, as its main properties are similar to those of LGS,[8-9] but its manufacturing is much easier.

*mero@mbi-berlin.de,§heinerzs@hu-berlin.de

The nonlinear coefficients and the Sellmeier equations of LGS[10,11] and BGS[12,13] were determined and predicted unique phase matching properties of these crystals when employed in OPA's pumped at 1 µm. It turned out that at a unique seed wavelength, broadband phase matching is possible in collinear geometry in these crystals leading to angular-dispersion-free, few-cycle MIR idler pulses with passively stabilized carrier-envelope phase (CEP). An additional advantage, predicted by the Sellmeier equations, is the near perfect group velocity matching of all three waves making it possible to use long nonlinear crystals without significant temporal pump walk-off. Yb-laser-pumped few-cycle LGS-based MIR OPA's pumped at 1 µm have already been demonstrated and reached the µJ level.[14,15] However, BGS has so far not been employed in ultrafast MIR OPA's.

Nonlinear optical properties of order higher than two (e.g., nonlinear refractive index due to the Kerr-effect, two-photon absorption coefficient) or charge drift and diffusion-based optical nonlinearities (e.g., photorefractive effect) are typically not investigated or considered in the design of ultrashort-pulse-pumped, high-repetition-rate OPA's. Here, we present our results on such nonlinear optical properties of oxide ($LiNbO_3$, $KTiOAsO_4$) and non-oxide ($LiGaS_2$, $BaGa_4S_7$) crystals and the corresponding 100-kHz, ultrafast SWIR/MIR OPA's based on these materials. In particular, we directly compare PPLN with KTA regarding their performance in the booster amplifier of a two-stage, dual-beam OPA at 1.5 and 3.2 µm. In addition, we describe an OPCPA delivering multi-GW peak power in two optically synchronized beams at 1.55 and 3.1 µm with a total average power of 55 W. Finally, we report on, for the first time, a BGS-based few-cycle MIR OPA and directly compare its performance to an LGS-based few-cycle MIR OPA.

2. METHODS

2.1 Z-scan measurements

In order to characterize the nonlinear refractive index and multi-photon absorption coefficient of OPA crystals at 1 µm, and identify the threshold of photorefractive damage, we employed the z-scan method.[16] Pulses from a commercial Yb:KGW laser probed the samples. The pulse duration was 180 fs and the laser repetition rate was adjustable up to 100 kHz. A camera was used to record the laser beam profile transmitted through the sample and the open and closed-aperture curves were obtained by numerical processing of the image files. All our measurements were conducted at two repetition rates: (i) 100 Hz to avoid thermo-optic effects and (ii) 100 kHz to mimic the conditions of the MIR OPA's. To include possible cascaded $\chi^{(2)}$: $\chi^{(2)}$ effects the way they may occur in an OPA, all crystals were cut for optical parametric amplification at a pump wavelength of 1 µm. Further details about the z-scan setup are provided elsewhere.[17]

In prior literature, the measurement of the nonlinear refractive index of z-cut KTA at a wavelength of 0.8 µm and a repetition rate of 76 MHz yielded $n_2 = 1.7\times10^{-15}$ cm^2/W.[18] Our KTA crystal was anti-reflection-coated, 4 mm long, and was cut for type-II phase matching in the XZ plane. We obtained $n_2 = 1.5\times10^{-15}$ cm^2/W at 100 Hz and 1.03 µm, for both ordinary and extraordinary polarization. The retrieved values were constant within error bars in the intensity range of 15-60 GW/cm^2.[17] However, starting already at 60 GW/cm^2 (peak intensity) and increasing in magnitude at higher intensities and at 100 kHz, we observed the signature of multi-photon absorption in the open-aperture traces (i.e., dip in transmission near the focal plane, $z = 0$) with an increasing contribution of possibly photorefractive effects at even higher intensities. Figure 1(a) and 1(b) show the transmitted beam profiles measured at a position z corresponding to the minimum in the closed-aperture traces at peak intensities of 60 and 120 GW/cm^2, respectively. The beam profiles show almost negligible difference between 100 Hz and 100 kHz when the peak intensity was 60 GW/cm^2 (Fig. 1(a)), although multi-photon absorption losses were already at the several % level (Fig. 1(c)). Increasing the repetition rate from 100 Hz to 100 kHz led to higher losses, possibly due to processes related to defect dynamics in the material. At a peak intensity of 120 GW/cm^2, the distortions in the transmitted beam profile were significant even at a repetition rate of 100 Hz (Fig. 1(b)). At 100 kHz, the beam profile was drastically distorted and showed a diffraction pattern characteristic of photorefractive effects. The dips in the corresponding open-aperture traces reached the multi-10 % level (Fig. 1(d)) with a functional dependence that cannot be explained by multi-photon absorption mechanisms alone. The strong light scattering by the sample at 120 GW/cm^2 was emitted in a large solid angle and some of the scattered light did not reach the detector. As a result, light scattering at 120 GW/cm^2 may have significantly contributed to the dip in the open-aperture traces hindering the extraction of multi-photon absorption coefficients. Even at 120 GW/cm^2 and 100 kHz, the transmitted beam profile recovered to the original, undistorted profile within seconds after blocking the laser beam in accordance with the contribution of photorefractive effects in this laser parameter range.

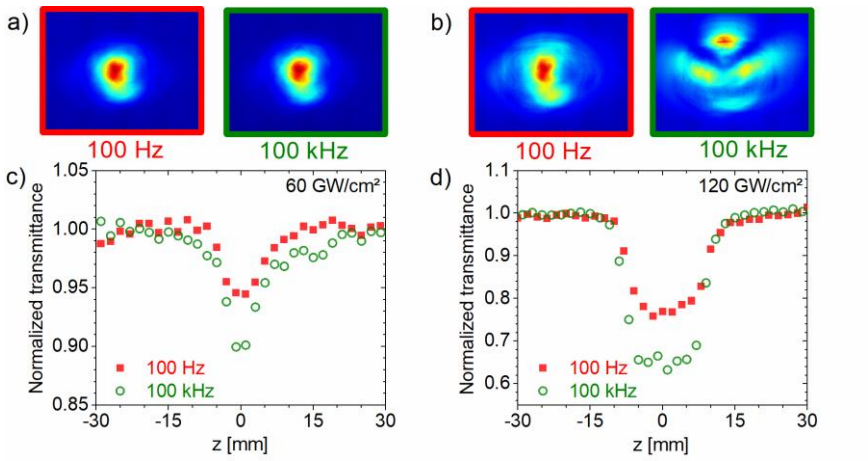

Figure 1. Transmitted beam profiles measured at a position z corresponding to the minimum in the closed-aperture traces at peak intensities of 60 GW/cm^2 (a) and 120 GW/cm^2 (b), at a repetition rate of 100 Hz (red boundary) and 100 kHz (green boundary). Open-aperture z-scan traces at a peak intensity of 60 GW/cm^2 (c) and 120 GW/cm^2 (d), at 100 Hz (solid red squares) and 100 kHz (open green circles). The 1-μm laser pulses were polarized in the XZ plane of KTA.

In a previous work,[17] we reported for the first time n_2 values for oriented LGS and unoriented BGS crystals at 1 μm. To test the stability of values from different manufacturers and growth runs, we repeated the measurements for longer samples oriented for optical parametric amplification in the MIR. The LGS sample was 8.0 mm long, uncoated, and was cut for type-I phase matching in the XZ plane. The BGS sample was 8.3 mm long, uncoated, and was also cut for type-I phase matching in the XZ plane. Figure 2 shows the closed- and open-aperture z-scan traces obtained for the two materials at 100 kHz with the laser radiation polarized in the XZ plane. We obtained $n_2 = 4.2\times10^{-14}$ cm^2/W for LGS, which agrees well with the values determined earlier for a shorter sample.[17] For BGS, we measured $n_2 = 1.0\times10^{-14}$ cm^2/W, which was 30-35% higher than the values we determined for the shorter, unoriented samples received from a different manufacturer.[17] At a peak intensity of only 2.3 GW/cm^2, we did not observe two- or three-photon absorption (Fig. 2, right panel). For both materials, the extracted n_2 values at 100 Hz were the same within error bars as those at 100 kHz.

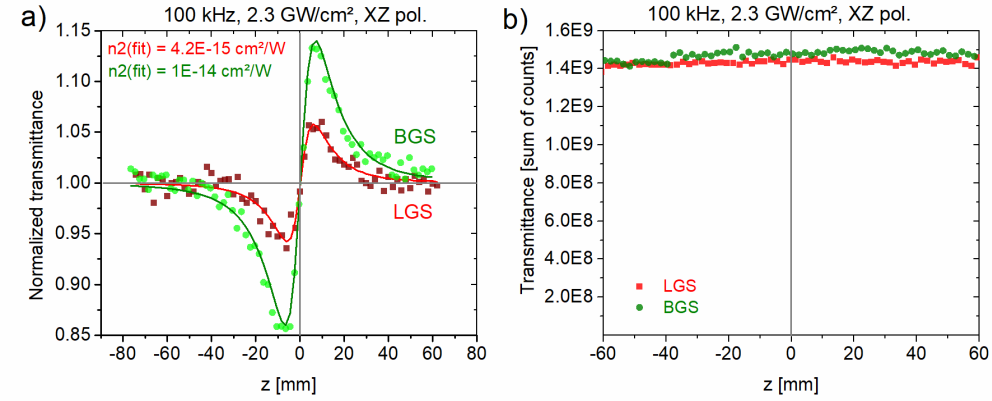

Figure 2. Closed-aperture (a) and open-aperture (b) z-scan traces obtained for uncoated 8.0-mm-long LGS (red symbols and line) and 8.3-mm-long BGS (green symbols and line) crystals cut for optical parametric amplification. The laser peak, on-axis intensity and repetition rate were 2.3 GW/cm^2 and 100 kHz, respectively. The solid lines are from modeling, yielding the fit values for n_2 shown in (a). The 1-μm laser pulses were polarized in the XZ plane.

2.2 Performance of PPLN and KTA in a dual-beam, ultrafast MIR OPA

To perform a head to head comparison between PPLN and KTA, we constructed a two-stage OPA, where one could switch between a PPLN- and a KTA-based second stage.[19,20] A pulse energy of 40 µJ (average power of 4 W) from a 180-fs, 100-kHz Yb:KGW laser was utilized to generate seed pulses in the 1.4-1.7-µm range and to pump the first and second OPA stages. The seed pulses were obtained though supercontinuum generation by focusing a small part of the pump pulses into a YAG window. The high-gain pre-amplifier was a 1-mm-long 5% MgO-doped PPLN crystal. The 1.5-µm output pulses from the PPLN-based first stage and the pump pulses of the second stage could be rerouted using removable mirrors to either a collinear, 2-mm-long PPLN or a noncollinear, 2-mm-long KTA crystal. Due to the lower effective nonlinear coefficient, d_{eff}, of KTA compared to PPLN, the beam waist of the pump pulses was adapted to ensure sufficient pump intensities to saturate the second stage. As the KTA-based second-stage was noncollinear, the MIR idler pulses emerging from it were angularly dispersed. Therefore, for the KTA-based OPA, we implemented a simple angular dispersion compensation setup[20] for the 3.1-µm idler beam at losses below 25%. This enabled dual-beam operation of even the noncollinear KTA OPA and a comparison of crystal performance at both 1.5 and 3.2 µm.

We observed improved performance of the two-stage OPA relying on KTA in the second stage.[19,20] Importantly, the KTA-based solution provided significantly higher conversion efficiency at better beam quality than the PPLN-based solution. The chirp-compensated average output power with KTA was 780 mW at 1.5 µm and 230 mW at 3.2 µm, while we obtained only 460 mW at 1.5 µm and 180 mW at 3.2 µm with PPLN. Figure 3 shows the temporal and spectral intensity and phase of the chirp-compensated 3.2-µm pulses (PPLN: Fig. 3(a) and 3(c); KTA: Fig. 3(b) and 3(d)) and the CEP jitter as a function of time (PPLN: Fig. 1(e); KTA: Fig. 1(f)). As demonstrated by the data in Fig. 3, KTA not only provided higher output pulse energies than PPLN, but also shorter pulses and lower CEP jitter. The pulse duration and CEP jitter with PPLN and KTA were 63 fs and ~300 mrad, and 53 fs and ~50 mrad, respectively. We attributed the inferior CEP jitter performance and beam quality of the PPLN-based booster amplifier compared to KTA to stronger photorefractive effects in PPLN than in KTA.

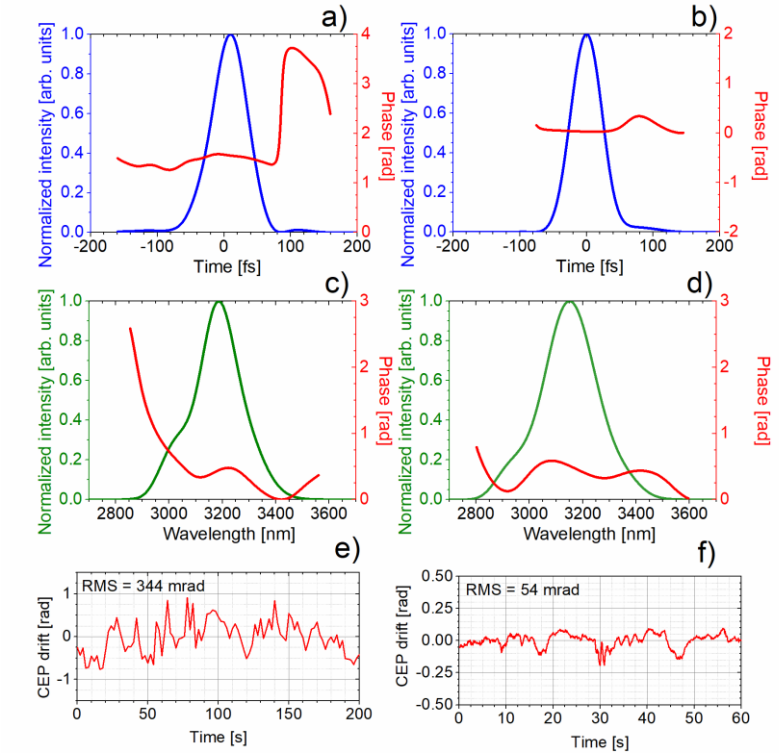

Figure 3. (a)-(d) Temporal and spectral intensity and phase measured using second-harmonic generation frequency resolved optical gating (SHG-FROG) for the 3.2-µm output beam, PPLN: (a) and (c), KTA: (b) and (d). Time-dependent CEP jitter measured using f-2f spectral interferometry for the 3.2-µm output of the PPLN-based (e) and the KTA-based (f) booster OPA. The PPLN crystal was heated to 150 C° to improve beam quality and performance. The KTA crystal was at room temperature.

Based on the results of our z-scan measurements and the comparison of the performance of PPLN and KTA, we chose KTA for the booster amplifier stages for the large-scale OPCPA system at the Max Born Institute. The system was developed for laser-driven electron rescattering and soft X-ray transient absorption experiments, and therefore, required average powers above 10 W at multi-GW peak powers both at 1.55 and 3.1 µm.[3] The seed pulses were obtained from a commercial two-branch Yb-fiber laser. The first branch was fiber-coupled and delivered stretched, 900 ps-long pulses at an energy of a few 10 nJ to seed a commercial Yb:YAG amplifier system. The second branch of the fiber laser drove a home-built white-light-seeded optical parametric amplifier (OPA0) based on BBO that was pumped at 515 nm. The 180 nJ, 1.55 µm, passively CEP-stabilized idler output of OPA0 served as the seed of OPCPA's OPA1-3. The first OPCPA stage (OPA1) was based on PPLN, while the booster amplifiers were based on KTA used in a non-collinear geometry. The peak pump intensity in the KTA stages was 70 GW/cm^2 and the crystals were placed behind the beam waists to ensure diverging wave fronts. The angular dispersion of the 3.1 µm idler pulses was compensated using a scheme described elsewhere.[20] The output consisted of 430 µJ, ~50 fs, 1.55 µm, CEP-stable pulses to drive high-harmonic generation (HHG) and 125 µJ, ~70 fs, 3.1 µm pulses. The high stability of the 1.5-µm beamline over a 1-hour period was confirmed by measuring the rate of generation of Ar^+ through the nominally 20-photon ionization process using a so-called cold target recoil ion momentum spectrometer (COLTRIMS).[3]

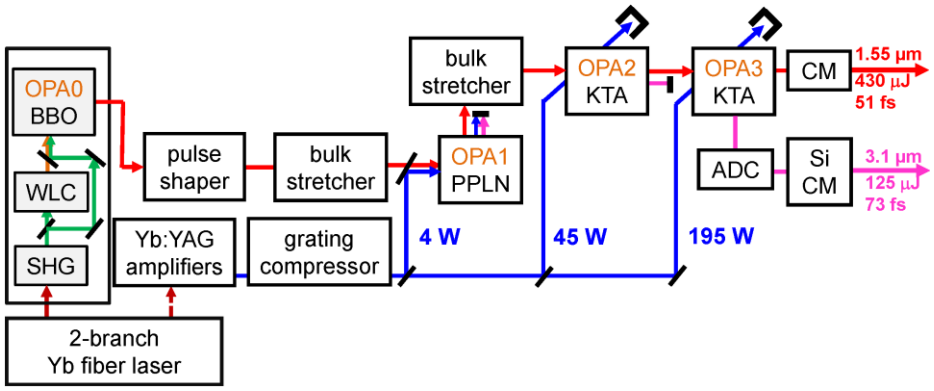

Figure 4. Scheme of the 100 kHz OPCPA system: A modified version of Fig. 1 from a previous publication[20] was reused (licensed under CC BY 4.0, https://doi.org/10.1364/OL.43.005246); SHG, second-harmonic generation; WLC, white-light continuum generation; OPA0-OPA3, optical parametric amplifiers based on BBO, PPLN, KTA, KTA, respectively; CM, chirped mirrors; ADC, angular dispersion compensation; Si, silicon window.

2.3 Performance of LGS and BGS in a single-beam, ultrafast MIR OPA

The Sellmeier equations of LGS predict two possibilities for broadband collinear phase matching: type-I phase matching in the XZ plane at an idler center wavelength of 7.8 µm (d_{eff} = -4.5 pm/V) and type-II phase matching in the XY plane at 8.6 µm (d_{eff} = 5.6 pm/V). The predicted configuration for BGS is type-I phase matching in the XZ plane at 8.7 µm (d_{eff} = 5.0 pm/V). For our OPA tests, we used the 8.0-mm-long LGS crystal (type-I, XZ plane, θ = 48.2°) and the 8.3-mm-long BGS crystal (type-I, XZ plane, θ = 13.1°) that were characterized in Section 2.1.

A 100-kHz, single-stage, white-light-seeded OPA was constructed for the comparison. The scheme of the OPA was similar to that in our prior work employing a 5-mm-long LGS crystal (type-I, XZ plane, θ = 48.2°).[14] Without changing the focusing conditions, either the LGS or the BGS sample was placed in the holder to perform the tests. Anti-reflection-coated germanium windows were used to compress the MIR idler pulses. Pump pulse energies up to 34 µJ were available. The pump beam was focused onto the crystals with diverging wave front at peak intensities up to 13 GW/cm^2. The LGS crystal could be pumped at maximum energies and delivered an output average power up to 58 mW at 8.0 µm, measured behind the germanium-based compressor. In contrast, the highest idler output average power measured after the germanium compressor for the BGS crystal was only 32 mW at 10.0 µm. The BGS crystal could not be pumped at energies above 32 µJ without a drop in the output power that could not be recovered by angle tuning of the crystal. Thermal dephasing was observed for BGS at pump pulse energies above 30 µJ. Figure 5(a) shows the average power from the LGS and BGS OPA's as a function of idler wavenumber / wavelength, while Fig. 5(b) shows the spectra measured at the highest output powers. In contrast to the predictions based on existing Sellmeier equations of BGS, we obtained the highest power at 10 µm and not 8.6 µm.

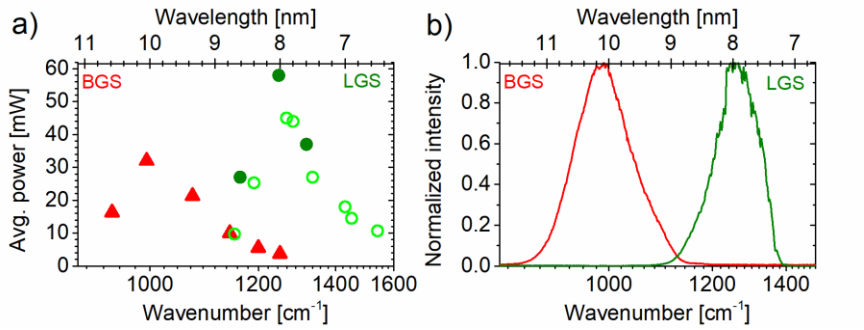

Figure 5. (a) Average power as a function of center wavelength measured for the chirp-compensated idler pulses and (b) idler spectra corresponding to the highest average powers, green: LGS, red: BGS. The spectral tuning performance shown by the open green circles in (a) was measured for a 5-mm-long LGS-based OPA.[14]

Cross-correlation frequency-resolved optical gating (X-FROG) was used to characterize the temporal shape of the idler pulses behind the germanium-based compressors. The reconstructed temporal intensities are shown in Fig. 6 for the LGS OPA at 8.0 µm and the BGS OPA at 10.0 µm. The pulse duration at full width at half maximum was 121 fs for LGS and 135 fs for BGS.

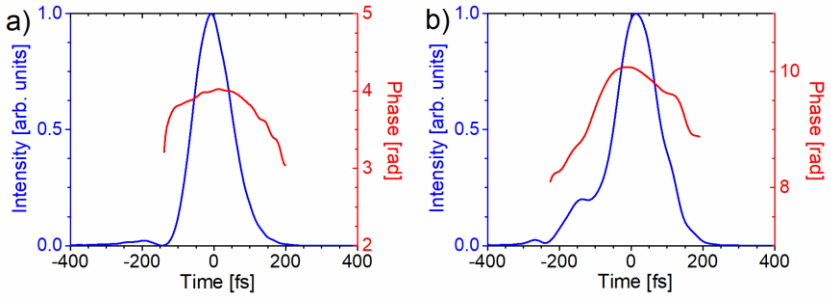

Figure 6. Reconstructed temporal intensity profiles obtained from cross-correlation frequency-resolved optical gating (X-FROG) for the LGS (a) and BGS (b) OPA at a center wavelength of ~8.0 µm and ~10.0 µm, respectively.

3. CONCLUSIONS

We investigated nonlinear optical properties of order higher than two (e.g., nonlinear refractive index due to the Kerr-effect, multi-photon absorption coefficient) and possible charge drift and diffusion-based optical nonlinearities (e.g., photorefractive effect) in oxide ($LiNbO_3$, $KTiOAsO_4$) and non-oxide ($LiGaS_2$, $BaGa_4S_7$) crystals. We found that KTA offers better overall performance in 1-µm-pumped MIR OPA's than PPLN. We compared the performance of LGS with BGS for the first time. BGS showed signs of thermal dephasing possibly due to multi-photon absorption of the 1-µm pump pulses and/or multi-phonon absorption near 10 µm. Nevertheless, the available crystal sizes for $LiGaS_2$ and $BaGa_4S_7$ hold great promise for few-cycle MIR OPA's scalable to an average power well above 1 W at pulse energies >> 10 µJ.

ACKNOWLEDGMENTS

We gratefully acknowledge funding from the Leibniz-Gemeinschaft under grant no. SAW-2012-MBI-2, the European Union's Horizon 2020 research and innovation programme under grant agreement no. 654148 Laserlab-Europe, the Deutsche Forschungsgemeinschaft (DFG) grant no. GSC 1013 SALSA and PE 607/14-1. Z.H. acknowledges funding by a Julia Lermontova Fellowship from DFG, No. GSC 1013 SALSA.

REFERENCES

[1] Elu, U., Baudisch, M., Pires, H., Tani, F., Frosz, M. H., Köttig, F., Ermolov, A., Russel, P. St. J., and Biegert, J., "High average power and single-cycle pulses from a mid-IR optical parametric chirped pulse amplifier," Optica 4(9), 1024-1029 (2017).

[2] Thiré, N., Maksimenka, R., Kiss, B., Ferchaud, C., Gitzinger, G., Pinoteau, T., Jousselin, H., Jarosch, S., Bizouard, P., Di Pietro, V., Cormier, E., Osvay, K., and Forget, N., "Highly stable, 15 W, few-cycle, 65 mrad CEP-noise mid-IR OPCPA for statistical physics," Opt. Express 26(21), 26907-26915 (2018).

[3] Mero, M., Heiner, Z., Petrov, V., Rottke, H., Branchi, F., Thomas, G. M., and Vrakking, M. J. J., "43 W, 1.55 μm and 12.5 W, 3.1 μm dual-beam, sub-10 cycle, 100 kHz optical parametric chirped pulse amplifier," Opt. Lett. 43(21), 5246-5249 (2018).

[4] Windeler, M. K. R., Mecseki, K., Miahnahri, A., Robinson, J. S., Fraser, J. M., Fry, A. R., and Tavella, F., "100 W high-repetition-rate near-infrared optical parametric chirped pulse amplifier," Opt. Lett. 44(17), 4287-4290 (2019).

[5] Bigler, N., Pupeikis, J., Hrisafov, S., Gallmann, L., Phillips, C. R., and Keller, U., "High-power OPCPA generating 1.7 cycle pulses at 2.5 μm," Opt. Express 26(20), 26750-26757 (2018).

[6] Petrov, V., "Frequency down-conversion of solid-state laser sources to the mid-infrared spectral range using non-oxide nonlinear crystals," Prog. Quantum. Electron. 42, 1-106 (2015).

[7] Isaenko, L., Yelisseyev, A., Lobanov, S., Krinitsin, P., Petrov, V., and Zondy, J.-J., "Ternary chalcogenides $LiBC_2$ (B = In, Ga; C = S, Se, Te) for mid-IR nonlinear optics," J. Non-Cryst. Solids 352, 2439-2443 (2006).

[8] Lin, X., Zhang, G., and Ye, N., "Growth and characteristics of $BaGa_4S_7$: A new crystal for mid-IR nonlinear optics," Cryst. Growth Des. 9(2), 1186-1189 (2009).

[9] Guo, Y., Zhou, Y., Lin, X., Chen, W., and Ye, N., "Growth and characterization of $BaGa_4S_7$ crystal," Opt. Mater. 36(12), 2007-2011 (2014).

[10] Petrov, V., Yelisseyev, A., Isaenko, L., Lobanov, S., Titov, A., and Zondy, J.-J., "Second harmonic generation and optical parametric amplification in the mid-IR with orthorhombic biaxial crystals $LiGaS_2$ and $LiGaSe_2$," Appl. Phys. B 78, 543-546 (2004).

[11] Kato, K., Miyata, K., Isaenko, L., Lobanov, S., Vedenyapin, V., and Petrov, V., "Phase-matching properties of $LiGaS_2$ in the 1.025–10.5910 μm spectral range," Opt. Lett. 42(21), 4363-4366 (2017).

[12] Badikov, V., Badikov, D., Shevyrdyaeva, G., Tyazhev, A., Marchev, G., Panyutin, V., Noack, F., Petrov, V., and Kwasniewski, A., "$BaGa_4S_7$: wide-bandgap phase-matchable nonlinear crystal for the mid-infrared, " Opt. Mater. Express 1(3), 316-320 (2011).

[13] Umemura, N., Petrov, V., Badikov, V. V., and Kato, K., "Temperature-tuned 90° phase-matched SHG and DFG in $BaGa_4S_7$," Proc. SPIE 9347, 93470N (2015).

[14] Heiner, Z., Wang, L., Petrov, V., and Mero, M., "Broadband vibrational sum-frequency generation spectrometer at 100 kHz in the 950-1750 cm^{-1} spectral range utilizing a $LiGaS_2$ optical parametric amplifier," Opt. Express 27(11), 15289-15297 (2019).

[15] Qu, S., Liang, H., Liu, K., Zou, X., Li, W., Wang, Q. J., and Zhang, Y., "9 μm few-cycle optical parametric chirped-pulse amplifier based on $LiGaS_2$," Opt. Lett. 44(10), 2422-2425 (2019).

[16] Sheik-Bahae, M., Said, A. A., Wei, T.-H., Hagan, D. J., and Van Stryland, E. W., "Sensitive measurement of optical nonlinearities using a single beam," IEEE J. Quantum Electron. 26(4), 760-769 (1990).

[17] Mero, M., Wang, L., Chen, W., Ye, N., Zhang, G., Petrov, V., and Heiner, Z., "Laser-induced damage of nonlinear crystals in ultrafast, high-repetition-rate, mid-infrared optical parametric amplifiers pumped at 1 μm," Proc. SPIE 11063, 1106307 (2019).

[18] Li, H. P., Kam, C. H., Lam, Y. L., and Ji, W., "Femtosecond z-scan measurements of nonlinear refraction in nonlinear optical crystals," Opt. Mater. 15(4), 237-242 (2001).

[19] Heiner, Z., Petrov, V., and Mero, M., "Compact, high-repetition-rate source for broadband sum-frequency generation spectroscopy," APL Photonics 2(6), 066102 (2017).

[20] Heiner, Z., Petrov, V., Steinmeyer, G., Vrakking, M. J. J., and Mero, M., "100-kHz, dual-beam OPA delivering high-quality, 5-cycle angular-dispersion-compensated mid-infrared idler pulses at 3.1 μm," Opt. Express 26(20), 25793-25804 (2018).

Title:

Progress in ultrafast, mid-infrared optical parametric chirped pulse amplifiers pumped at 1 μm

Authors:

Mark Mero, Valentin Petrov, Zsuzsanna Heiner

Manuscript

The original publication may be found at:

Journal: Proc. SPIE 11264, Nonlinear Frequency Generation and Conversion: Materials and Devices XIX, 112640F (2 March 2020)

DOI: https://doi.org/10.1117/12.2545961

Copyright 2020 Society of Photo-Optical Instrumentation Engineers (SPIE). One print or electronic copy may be made for personal use only. Systematic reproduction and distribution, duplication of any material in this paper for a fee or for commercial purposes, or modification of the content of the paper are prohibited.